Recent changes in drainage route and outburst magnitude of Russell Glacier ice-dammed lake, West Greenland

Mads Dømgaard[1], Kristian K. Kjeldsen[2], Flora Huiban[1], Jonathan L. Carrivick[3], Shfaqat A. Khan[4], Anders A. Bjørk[1]

[1]Department of Geoscience and Natural Resource Management, University of Copenhagen, 1350 Copenhagen K, Denmark
[2]Geological Survey of Denmark and Greenland (GEUS), 1350, Copenhagen K, Denmark
[3]School of Geography and water@leeds, University of Leeds, Woodhouse Lane, Leeds, LS2 9JT, UK
[4]DTU Space – National Space Institute, Technical University of Denmark, Kgs. Lyngby, Denmark

10 *Correspondence to*: Mads Dømgaard (mld@ign.ku.dk)

Abstract. Glacial lake outburst floods (GLOFs) or 'jökulhlaups' from ice-dammed lakes are frequent in Greenland and can influence local ice dynamics, bedrock displacement, geomorphological changes and flooding hazards. Multidecadal time series of lake drainage dates, drainage volumes and flood outlets are rare but essential for understanding the impact on and interaction with the surroundings, identifying drainage mechanisms, and for mitigating downstream flood effects. In this study, we use ultra-high-resolution structure-from-motion (SfM) digital elevation models (DEM) and orthophotos from unmanned aerial vehicle field surveys in combination with optical satellite imagery to reconstruct robust lake volume changes associated with 14 GLOFs between 2007 and 2021 at Russell Glacier, West Greenland. This makes it one of the most comprehensive and longest records of ice-dammed lake drainages in Greenland. We find a mean difference of 10 % between the lake drainage volumes compared with estimates derived from a gauged hydrograph 27 km downstream. Due to ice dam thinning, the potential maximum drainage volume in 2021 is c. 60 % smaller than that estimated to have drained in 2007. Our time series reveals variations in the drainage dates ranging from late May to mid-September and moreover that drained volumes range between 0.9 - 37.7 M m^3. We attribute these fluctuations between short periods of relatively high and low drainage volumes to a weakening of the ice dam and an incomplete sealing of the englacial tunnel following the large GLOFs. The syphoning drainage mechanism is triggered by a reduction in englacial meltwater, likely driven by late seasonal drainages and sudden temperature reductions, as well as annual variations in the glacial drainage system. Furthermore, we provide geomorphological evidence of an additional drainage route first observed following the 2021 GLOF with a sub- or englacial and supraglacial water flow across the ice margin. It seems probable that the new drainage route will become dominant in the future which will drive changes in the downstream geomorphology and raise the risk of flooding-related hazards as the existing buffering outlet lakes will be bypassed.

30

1 Introduction

Ice-dammed lakes can form either in supraglacial, subglacial or ice-marginal positions (Tweed and Russell, 1999). Globally, proglacial lakes (including ice-marginal lakes) contain up to 0.43 mm of sea level equivalent (Shugar et al., 2020) and recent studies show that ice-marginal lakes in Greenland have increased in number and size (Carrivick and Quincey, 2014; Shugar et
35 al., 2020). More than 3300 ice-marginal lakes are found in Greenland, mostly around peripheral mountain glaciers and ice caps (PGICs) but there is also a relatively high density of ice-dammed lakes along the southwest Greenland ice sheet (GrIS) margin (Carrivick et al., 2022; How et al., 2021). The outflow of ice-dammed lakes can vary substantially from a gradual near-steady discharge to sudden outburst floods called jökulhlaups or Glacial Lake Outburst Floods (GLOFs) (Tweed and Russell, 1999). Several mechanisms have been proposed for the rapid drainage of ice-dammed lakes and due to changes in lake inputs and
40 topographic settings, drainages at the same lake may be in response to different trigger mechanisms (Tweed and Russell, 1999). Sudden drainage of water from ice-dammed lakes in Greenland can have implications on fjord circulation (Kjeldsen et al., 2014), affect local ice dynamics (e.g. Kjeldsen et al., 2017; Sugiyama et al., 2007), cause bedrock displacements (Furuya and Wahr, 2005; Kjeldsen et al., 2017), alter downstream geomorphology (Russell et al., 2011) as well as have severe societal impacts (Carrivick and Tweed, 2016).
45 Carrivick and Tweed (2019) review the status of knowledge on GLOFs and ice-dammed lake drainages in Greenland and show that continuous multidecadal observation of transient lake water levels (i.e. pre- and post-drainage), lake drainage dates, and released flood volumes are extremely rare. Nevertheless, such time series are important for revealing spatio-temporal patterns in lake drainage and flood timings and magnitudes. Furthermore, long-term data improve our understanding of drainage triggers and mechanisms and helps in the mitigation of downstream effects. The primary aim of this paper is to (re)calculate
50 and analyse the lake water level and lake drainage volume of 14 historical GLOFs observed from 2007 to 2021. Secondly, we investigate geomorphological changes supporting a shift in the proglacial GLOF drainage route observed following the recent GLOF on August 22, 2021.

2 Study site

One of the most intensively monitored and studied ice-dammed lakes in Greenland is located on the northern flank of Russell
55 Glacier in West Greenland (Figure 1) (Carrivick et al., 2017; Lamsters et al., 2020; Mikkelsen et al., 2013; Russell, 1989, 2007; Russell et al., 2011) and so it is a key site for understanding GLOFs. The lake is ~0.7 km^2 and drains through a c. 600 to 1000 m glacial tunnel in the southwestern part of the lake transporting water and sediment into two outlet lakes and further into the Watson River (Carrivick et al., 2013; Carrivick et al., 2018; Mernild and Hasholt, 2009; Russell, 1989; Russell, 2007; Russell et al., 2011). Based on aerial photographs, sedimentary data and refill rates the lake drained every 2 to 3 years from
60 the 1950s and until 1987 where it entered a 20-year stagnant period of stable water level (Carrivick et al., 2018; Russell et al., 2011). On the 31st of August 2007 a new GLOF occurred (Russell et al., 2011) and the lake entered a new cycle of almost yearly reoccurring drainage events, with the last documented event happening in 2015 (Carrivick et al., 2017). Drainage

parameters of the lake at Russell Glacier have previously been estimated using a variety of different methods such as downstream gauged hydrographs, pressure transducers within the lake, time lapse cameras and Global Positioning System (GPS) using differential GPS (dGPS) technique to monitor water surface elevation (Carrivick et al., 2017; Mernild and Hasholt, 2009; Mikkelsen et al., 2013; Russell et al., 2011).
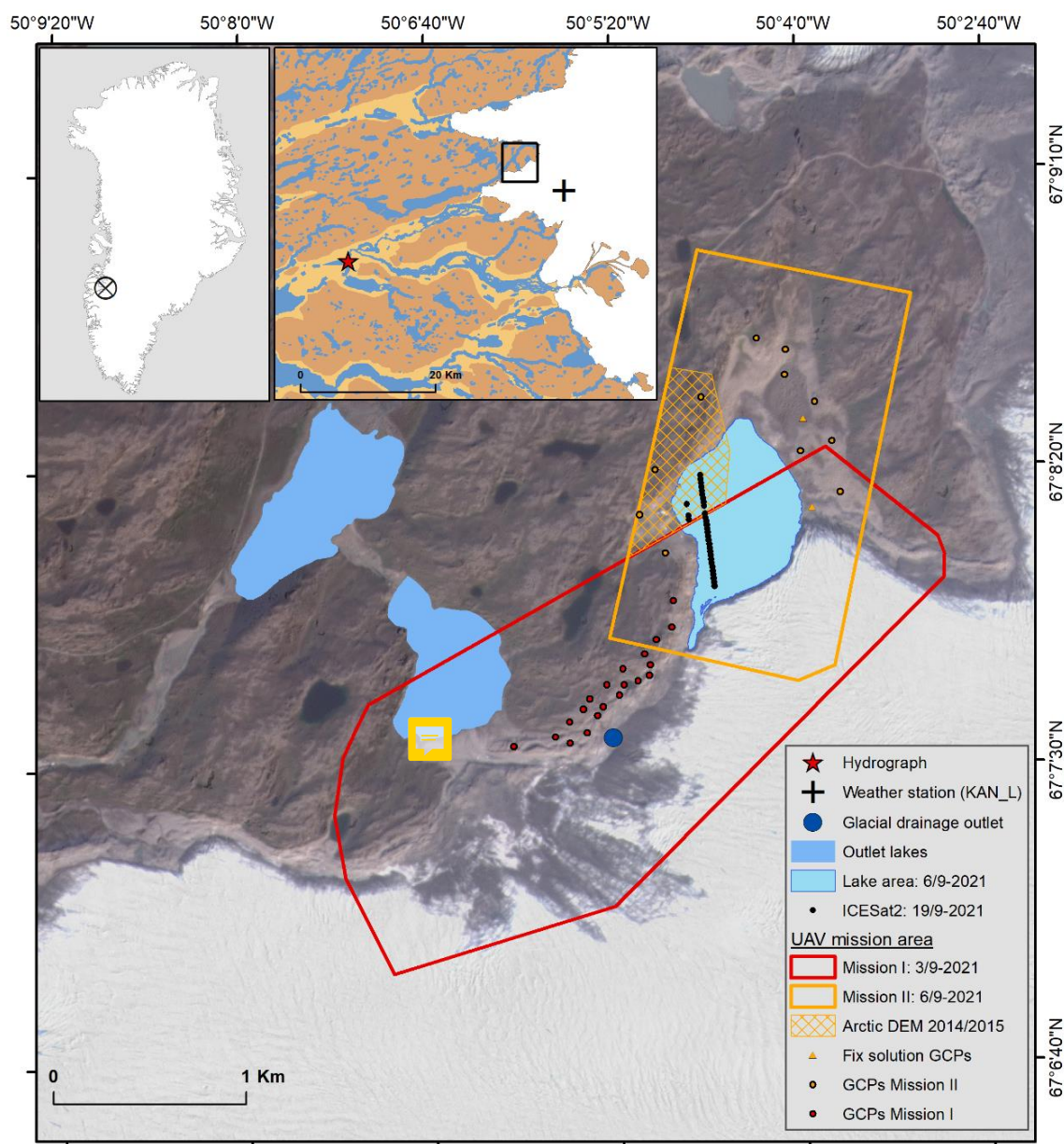
Figure 1. Study site location and UAV mission area shown on Planet (2017) imagery from 23/8-2021. Marked position of hydrograph and weather station (KAN_L) on overview map.

3 Methods and data

Fieldwork at Russell Glacier was carried out between the 3rd and 6th of September 2021, two weeks after a GLOF on 22nd
70   August 2021. Two UAV missions were conducted to produce DEMs and orthophotos of the drained lake basin topography,
ice margin and the outlet and flood drainage route (Figure 1). As the lake did not fully drain we were not able to capture the
entire drained lake topography. A minimum water level of 408.8 m was surveyed, which is almost identical to the minimum
lake levels observed after other previous GLOFs. Russell et al. (2011) produced a DEM of the lake basin bathymetry made
from interpolation of kinematic dGPS tracks surveyed in February 2008, with a minimum elevation of 410 m. In this study,
75   our UAV mission enabled a highly accurate and ultra-high-resolution DEM without surface interpolation. From the refined
UAV-derived DEM we can precisely estimate the pre- and post-GLOF water level, lake area and lake drainage volume of
historical and future events. All elevations are reported as height above the WGS84 ellipsoid, unless otherwise stated.

3.1 Aerial surveys

The UAV flights were conducted on two different dates using two different UAVs, due to the battery capacity and weather
80   conditions (Table 1, Figure 1):

Table 1 Overview of the two UAV mission. *Parentheses indicate the number of GCPs with a fixed GNSS solution

UAV Mission	Flight date	UAV type	Flight mode	Images captured	Covered area (km²)	Camera position accuracy (m)		Resolution (m)		Number of GCPs*	RMSE camera location (m)		
						Vertical	Horizontal	DEM	Ortho		X	Y	Z
Mission I	03-09-2021	Fixed-wing, WingtraOne w. PPK	Automatic	1106	4.3 (60% overlap)	0.06	0.09	0.1	0.036	20 (0)	0.01	0.01	0.02
Mission II	06-09-2021	Quadcopter, DJI Phantom 4 Pro w. PPK	Manual	563	2.39	0.06	0.09	0.1	0.1	13 (2)	0.28	0.32	0.14

Both UAVs have an onboard post-processed kinematic (PPK) GNSS receiver logging position data at the time of image
85   acquisition. This gives absolute centimeter-level accuracies in both the vertical and horizontal direction and removes the need
for ground control points (GCPs) (Chudley et al., 2019). The UAV PPK data was post-processed using WingtraHub (*v. 2.2.0*)
and KlauPPK (*v. 7.17*) software. We used base station data from the fixed Greenland GNSS Network (GNET) station located
in Kangerlussuaq (KLSQ) approx. 30 km from the field site (Bevis et al., 2012). The processed camera position has a vertical
and horizontal accuracy of c. 0.09 m and 0.06 m, respectively.

90

For the purpose of validating the accuracy of the produced DEMs we placed ground control points (GCPs) in each study area
and measured their position using an Emlid Reach RS2 GPS (Table 1). Due to poor satellite reception and cycle slips we were

only able to retrieve reliable fix solution position results for 0/20 and 2/13 GCPs in Mission I and Mission II, respectively (Table 1, Figure 1).

3.2 Development and validation of DEMs and orthophotos

The UAV images were processed using a structure-from-motion (SfM) workflow in Agisoft Metashape Pro. (*v. 1.7.4*). We follow the general processing workflow described in the official Agisoft guidelines (Agisoft LLC, 2020). The camera calibration is set as 'precalibrated' and the calibration parameters are set according to the calibration report of the used camera. The post-processed, geolocated camera positions are used as input instead of GCPs. During the bundle adjustment, we perform a refined camera calibration, which is recommended when other variables are well constrained (Chudley et al., 2019). Mission I DEM and orthophoto have a resolution of 0.1 x 0.1 m and 0.036 x 0.036 m, respectively. The Mission II DEM and orthophoto both have a resolution of 0.1 x 0.1 m (table 1). The RMSE of the X, Y and Z camera location after model generation is 0.01, 0.01, and 0.02 m for Mission I and 0.28, 0.32, and 0.14 m for Mission II (table 1). Based on the GCPs we were only able to estimate the accuracy of the Mission II DEM, which is found to be xy = 0.14 m and z = 0.35 m.

Due to image gaps at the western part of the lake, we were not able to produce a complete UAV-derived DEM of the drained lake topography. Thus, the missing parts were filled with elevation measurements from two Arctic DEM strips captured on the 2nd of August 2015 and 19th of September 2014, respectively (Figure 1). At the time of acquisition, both Arctic DEMs had a water level of approx. 407 m. The Arctic DEM strips have a resolution of 2 x 2 m and are based on photogrammetric processing of Worldview stereo-image pairs (Noh and Howat, 2015). We mainly use the 2015 DEM strip as it is produced from images acquired only 5 days after the 2015 drainage event. The 2015 DEM strip contains a few areas with no data, which we filled with values from the 2014 DEM strip produced from images captured 47 days after the 2014 drainage event. Prior to mosaicking, all DEMs were resampled to 0.1 m resolution and co-registered over solid bedrock using the python module PyBob (McNabb, 2019) based on the method developed by Nuth and Kääb (2011).

Using the mosaic of Mission II DEM and ArcticDEM as well as the Mission II orthophoto we digitize the lake area and estimate the water level on 6th September 2021 to 408.8 m ± 0.35, by extracting the elevation of points every 5 m along the digitized waterline at the eastern part of the lake. Finally, all elevation data within the lake area were changed to 408.8 m to avoid erroneous elevation estimates on the water surface. The final mosaicked and lake-burned DEM will be referred to as the 2021 post-drainage DEM. We validated the estimated water level by comparing it to 33 ICESat2 data points from 19th September 2021 measured at the interior of the lake (Figure 1). The ICESat2 points have a mean water level of 408.70 m and a STD of 0.02 m.

3.3 Estimation of water level, lake area and drainage volume

To estimate the lake water level at different timestamps we use satellite images from Planet scope, Landsat 7 and 8 and Sentinel-2. The satellite images were manually georeferenced to the high-resolution UAV orthophotos to adjust for small

125 offsets. Inspired by the approach of previous studies (Carrivick and Tweed, 2019) the pre- and post-drainage water level is determined by manually placing 30 points along the eastern part of the lake's waterline as observed on the satellite images, and then extracting the elevation at these points from the produced 2021 post-drainage DEM. The eastern part is chosen as it only contains high-resolution (0.1 x 0.1 m) UAV-derived elevation pixels as well as having a flat slope compared to the steep terrain in the west (Figure A1). Based on the 30 elevation points we calculate the mean water level and the standard deviation

130 indicating the uncertainty of the elevation estimate (Table 2). The mean water level is used to estimate the lake outline and area by masking out pixels above the mean water level as well as removing depressions not linked to the existing lake area. Using the estimated lake area and the 2021 post-drainage DEM we calculated the pre- and post-drainage water volumes using Eq. (1):

$$\sum_{i=1}^{n}(\mu_{wl} - P_{elev_i}) * P_{width_i} * P_{height_i}, \qquad (1)$$

135 where n denotes all pixels within the lake area, μ_{wl} the mean water level, P_{elev_i} the elevation of the pixel and P_{width_i} and P_{height_i} the pixel resolution, which is 0.1 x 0.1 m. The total lake area change and water volume release of every GLOF is determined by simply extracting the pre and post-drainage estimates (Table 2). As area and volume estimates are calculated relative to the 6th of September 2021 when images for the 2021 post-drainage DEM were acquired, they are sensitive to changes in the position of the ice margin. From 2007 to 2011 we have observed a gradual advance of the margin, while after 2011 the front

140 has been relatively stable with just slight changes (Figure A2). Thus, we adjust both the lake area and drainage volumes from 2007 to 2011 by manually expanding the lake area to match the position of the ice margin and assuming a similar water level change of the entire added area corresponding to the estimated pre- and post-drainage level.

All drainage estimates from 2017-2021 are based on Planet scope satellite images, whereas estimates of previous events are based on mainly panchromatic images from Landsat 7 and 8 with a resolution of 15 m as well as RGB images from Sentinel-

145 2 with a resolution of 10 m (table 2). In contrast to the low (10 and 16 days) temporal coverage of the Landsat and Sentinel images, Planet images not only have a much better spatial resolution of 3 m, but also a temporal resolution of approximately 1 day (Planet, 2017), enabling detection of sudden changes in water level, albeit during clear-sky conditions.

3.4 Drainage routes

Based on the Mission I derived DEM we determine the main surface drainage routes for the GLOF drainage water running

150 from the glacial drainage outlet to (i) the outlet lakes and (ii) across the ice margin. The drainages routes are calculated as the paths of least resistance from the source (drainage outlet) to the destinations (i and ii) assuming that water is flowing to the neighbouring pixel with the lowest elevation. The calculations are based on 2 x 2 m resampled version of the DEM to even out locale elevation maxima from small surface features such as rocks and ice blocks that potentially hinders the water flow. Finally, we generated points every two meters along both of the estimated drainage routes and extracted the underlying

155 elevations to determine each routes maximum elevation.

3.5 Hydrograph volume estimation

We estimated the drainage volume from a hydrograph station deployed in Watson River at Kangerlussuaq, 27 km downstream of the lake (van As et al., 2017). Here pressure transducers record changes in water pressure, which subsequently is corrected for atmospheric pressure before converted into hourly averages in water stage. Water discharge is obtained using rating curve,
160 based on discharge measurements at various water levels, and is an associated with a conservative uncertainty value of 15%. Due to diurnal fluctuation in discharge, induced by melting of the vast ice coverage in the catchment, we estimated the daily minima and maxima on the day of the drainage event, by fitting linear trend through the equivalent low and high stage values on the day before and after. This allowed estimates of the baseflow and thus estimates of the volume associated with lake drainage.

165 ## 3.6 Temperature data

The temperature record is obtained from the KAN_L Automatic Weather Station, which is part of the PROMICE AWS network, and is located on the ice sheet proper at 670 m asl. We use hourly average data that is based on measurements recorded every 10 min (Fausto et al., 2021; GEUS Dataverse n.d).

4 Results

170 ## 4.1 Drainage volumes

Figure 2 shows how the lake volume and area change with the water level as calculated based on the 2021 post-drainage DEM. The lake has a theoretical maximum water level of 433 m, after which water overspills the ice dam. The 2021 theoretical water level maximum produces a lake surface area of 0.79 km^2 and a maximum drainage volume of 14.3 M m^3. To accommodate a higher water level associated with the situation in 2007, we manually adjust the ice margin and thus the resulting volume.
175 Based on the present configuration of the lake and ice margin, the lake would likely never reach the 2007 maximum level as it would drain through the glacial conduit at a lower level. Moreover, we regard the theoretical maximum as a proxy for the thickness of the ice dam. From the 2015 Arctic DEM strip we determine a theoretical maximum water level of 450 m, giving a total lowering of 17 m compared to 2021.
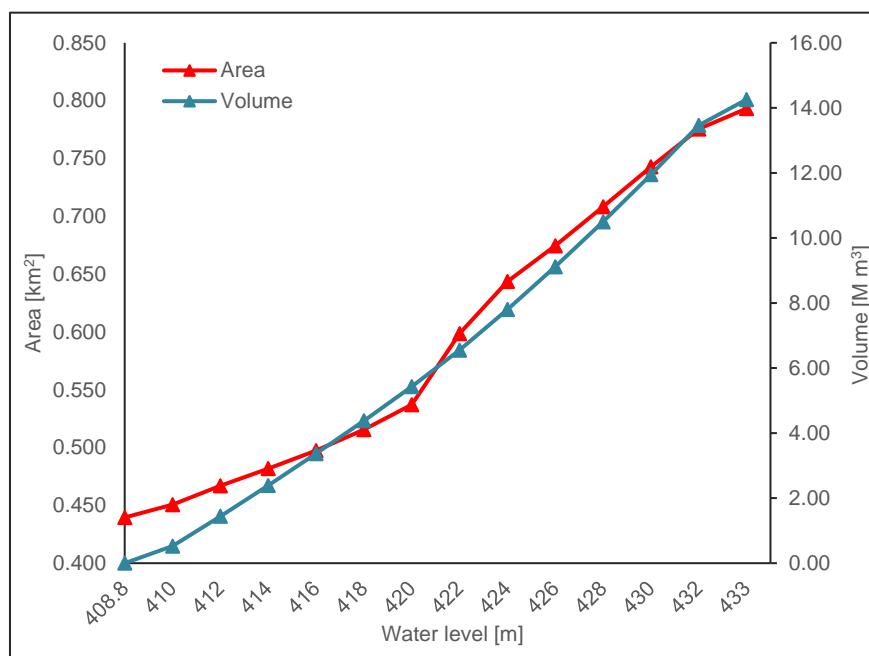
Figure 2. Relationship between water level and area (km²) and water level and volume (M m³), calculated based on the 2021 post-drainage DEM. The lake has a theoretical maximum water level of 433m after which it overspills.

180 **4.2 Drainage cycles**

Since the lake entered its new drainage cycle in 2007 we observe yearly reoccurring events, with the exception of 2009. The 2007 GLOF had the largest observed volume release of 37.73 ± 1.08 M m³ (Table 2 and Figure 3). In 2008 the volume release was four times lower at just 9.4 ± 1.46 M m³. No draining was observed in 2009, but in 2010 the release volume was much larger again at 26.08 ± 2.54 M m³. In the following three years (2011 to 2013) the volume released was relatively stable

185 between 7 and 9 M m³, whereas the 2014 and 2015 outburst volume decreased to ~4 M m³, after which a three times increase occurred to 12.5 M m³ in 2016. In both 2017 and 2020, we have reconstructed small, partial drainage events of just 2.7 and 0.9 M m³, respectively (Table 2 and Figure 3). These two events occurred earlier in the melt season compared to any previous drainages, with the 2020 event happening already on the 31st of May. In years after the observed partial drainage, i.e. in 2018 and 2021, the GLOFs then occurred relatively late in the melt season and with volumes of 8.5 and 9 M m³, respectively (Table

190 2 and Figure 3). In general, the lake seems to fluctuate between short periods of relatively high and low drainage volumes, with the low volume GLOFs happening earlier in the melt season. However, a later drainage date is not always equivalent to a larger drainage volume, as evident in 2018 and 2019.

195

Table 2. Drainage dates, pre- and post-drainage water level, lake area, and volume estimate from DEM method as well as volume estimates from hydrograph method. Includes references to previous studies of the lake

Drainage dates	Water level (m)		Lake area (km2)		Area change (km2)	Volume relative to 6th Sept. 2021 (M m3)		Lake volume release (M m3)	Source	Volume from hydrograph (M m3)	Other references and volume estimates (M m3)
	Pre drain	Post drain	Pre drain	Post drain		Pre drain	Post drain				
17-19. July 1987	450.8	402.5						31.3	Russell et al., 2011.		Russell 2007; Russell 1989
31. Aug. 2007	453.1 ± 0.9	< 408.8	1.308* ± 0.022	0.475* ± 0.007	0.833 ± 0.023	37.73** ± 1.08	0***	37.73 ± 1.08	This study (Landsat 7)	43.19 ± 6.47	Russell et al. 2011 (39.1 ± 0.8) Mikkelsen et al. 2013 (25.5) Mernild & Hasholt 2009 (11.3)
31. Aug. 2008	425.3 ± 2.2	< 408.8	0.710* ± 0.037	0.435* ± 0.008	0.275 ± 0.038	9.40** ± 1.46	0***	9.40 ± 1.46	This study (Landsat 7)	9.75 ± 1.46	Russell et al 2011 (12.9 ± 0.3) Mikkelsen et al. 2013 (3.6) Mernild & Hasholt 2009 (4.6)
11. Sept. 2010	445.7 ± 2.3	410.4 ± 1.3	1.051* ± 0.092	0.495* ± 0.013	0.556 ± 0.093	27.26** ± 2.33	1.18** ± 1.02	26.08 ± 2.54	This study (Landsat 7)	26.66 ± 4.00	Carrivick 2017 (30.7) Mikkelsen et al. 2013 (8.4)
14. Aug. 2011	421.3 ± 2.4	< 408.8	0.583* ± 0.057	0.413* ± 0.007	0.170 ± 0.057	6.90** ± 1.38	0***	6.90 ± 1.38	This study (Landsat 7)	8.02 ± 1.20	Carrivick et al .2017 (No vol.)
11. Aug. 2012	425.7 ± 1.1	< 408.8	0.670 ± 0.018	0.404* ± 0.008	0.266 ± 0.020	8.91 ± 1.29	0***	8.91 ± 1.29	This study (Landsat 7)	8.81 ± 1.32	Carrivick et al .2017 (25.5)
15. Sept. 2013	426.0 ± 2.0	< 408.8	0.674 ± 0.031	0.413* ± 0.007	0.261 ± 0.032	9.12 ± 1.35	0***	9.12 ± 1.35	This study (Landsat 8)	9.65 ± 1.45	
3. Aug. 2014	418.4 ± 2.0	< 408.8	0.519 ± 0.021	0.410* ± 0.007	0.109 ± 0.028	4.59 ± 1.04	0***	4.59 ± 1.04	This study (Landsat 8)	9.31 ± 1.40	Carrivick et al .2017 (8.0)
28. July 2015	417.4 ± 0.7	< 408.8	0.510 ± 0.006	0.411* ± 0.007	0.099 ± 0.009	4.07 ± 0.36	0***	4.07 ± 0.36	This study (Landsat 8)	4.22 ± 0.63	Carrivick et al .2017 (7.5)
8. Sept. 2016	430.8 ± 0.7	408.9 ± 0.3	0.748* ± 0.01	0.441 ± 0.003	0.307 ± 0.010	12.53 ± 0.51	0.04 ± 0.08	12.49 ± 0.52	This study (Sentinel-2)	11.78 ± 1.77	
7. July 2017	415.7 ± 0.5	410 ± 0.7	0.495 ± 0.004	0.451 ± 0.006	0.044 ± 0.007	3.22 ± 0.25	0.53 ± 0.32	2.69 ± 0.41	This study (Planet)	1.89 ± 0.28	
12-13. Sept. 2018	425.1 ± 1.0	< 408.8	0.661 ± 0.015	0.440* ± 0.007	0.221 ± 0.017	8.51 ± 0.66	0***	8.51 ± 0.66	This study (Planet)	No data	
31. Aug. 2019	429.7 ± 0.2	410.5 ± 0.4	0.732* ± 0.002	0.455 ± 0.002	0.277 ± 0.003	11.71 ± 0.15	0.75 ± 0.14	10.96 ± 0.21	This study (Planet)	10.00 ± 1.50	
31. May 2020	410.8 ± 0.4	< 408.8	0.457 ± 0.003	0.428* ± 0.007	0.029 ± 0.08	0.89 ± 0.18	0***	0.89 ± 0.18	This study (Planet)	0.75 ± 0.11	
22. Aug. 2021	425.7 ± 0.4	< 408.8	0.670 ± 0.006	0.438* ± 0.007	0.232 ± 0.009	8.91 ± 0.27	0***	8.91 ± 0.27	This study (Planet + UAV ortho)	8.22 ± 1.23	

* The areas are manually edited. From 2007-2011 to compensate for changes at the ice margin. Pre drain 2016 and 2019 to avoid water extending on the ice margin. Post drain 2012-2015, 2018 and 2020-2021 as the water level is lower than the reference minimum of 408.8 m

**Volumes adjusted to compensate for changes at the ice margin. We assume the water level changes from post drain to pre drain level for the entire added area

***The volume is set to 0 despite being slightly lower than the reference DEM. As the post drain area is close to the reference area (0.439 km2) the volumes are assumed to be almost identical

200
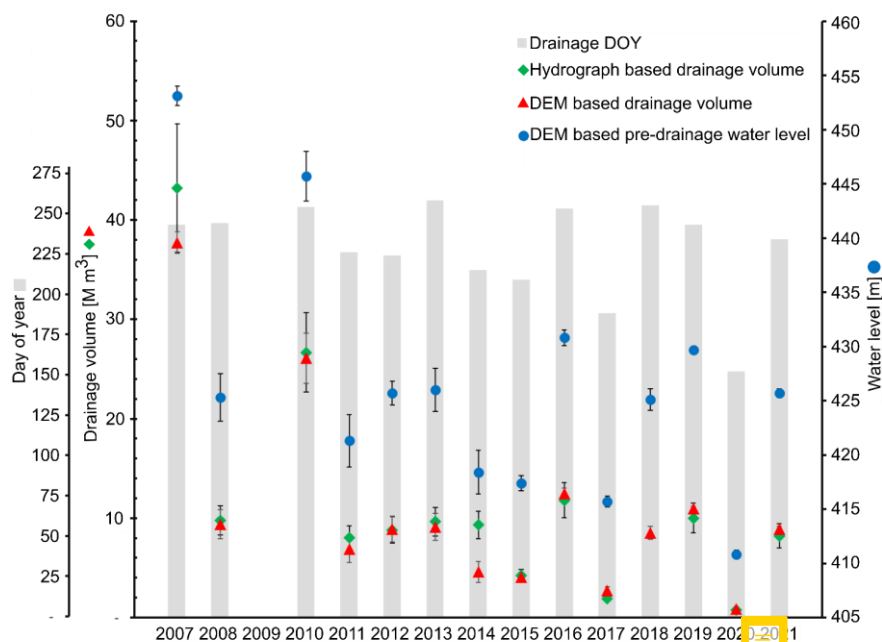
Figure 3. Drainage water level and drainage volume is reconstructed based on the DEM method and drainage volume from hydrograph methods. The grey bars indicate the day of year (DOY) of the drainage event. No hydrograph data for the 2018 event. Note that there is no relationship between the volume Y-axis and the water level Y-axis.

4.3 Geomorphological surface features of the drainage area

Figure 4A and 4B show the two main drainage routes for the GLOF drainage water exiting the glacial drainage outlet. Drainage route I channels the water into a proglacial passage and further into two outlet lakes connected to the downstream river network. Drainage route II leads the water across the ice margin and into an ice-marginal meltwater drainage system before reaching the river network, thus bypassing the two outlet lakes. There is a 0.4 m elevation difference between the drainage threshold of drainage route I (390.2m) and drainage route II (390.6m) (Figure 4B).

The 0.1 m resolution image in Fig. 4B is generated based on the Mission I derived DEM and shows the drainage area following the 2021 GLOF. The ultra-high-resolution of the hillshade, DEM, and orthophoto allows us to observe geomorphological features not visible in the high-resolution Planet satellite images (3 m). As evident, large blocks of ice up to 5 m x 5 m are observed scattered along both drainage route I and II (Figure 4B, 4C, 4D). On the western part of the ice margin we observe a c. 100 m x 100 m area where the ice surface is fractured and broken (Figure 4F). The ice margin also contains 0.5 m to 3 m wide, parallel, circular cracks that run up to several hundred meters (Figure 4B, 4G, 4H), as well as five water escape holes with a diameter of c. 10 m (Figure 4E). Observations of the 2015 and 2021 positions of the ice margin and glacial drainage outlet show a 30 m and 60 m retreat, respectively (Figure 4B).
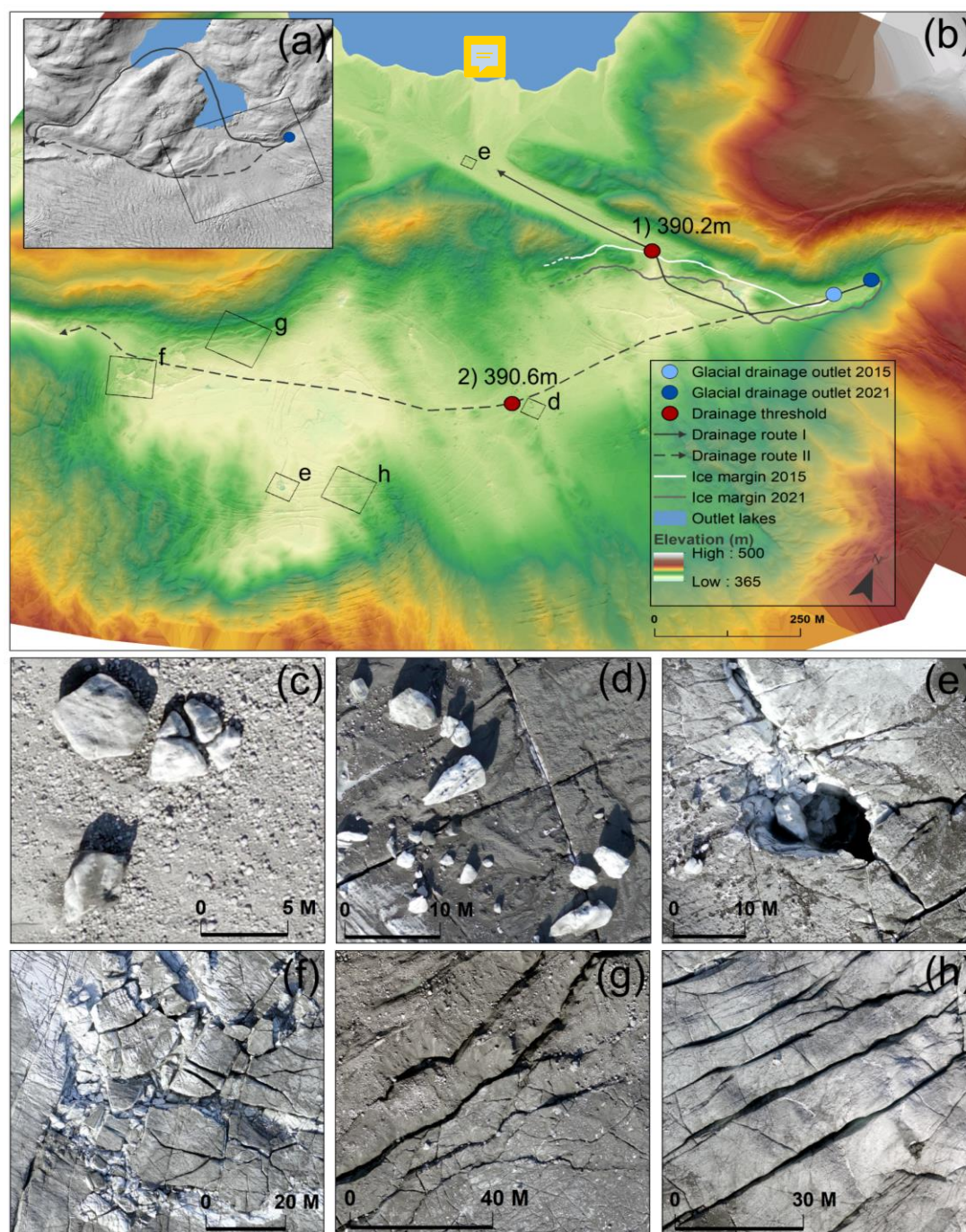
Figure 4. A) Overview of drainage route I and II overlaid on a hillshade based on the ArcticDEM from 2nd *Aug.* 2015 (with a marked zoom in of area b). B) Color-coded hillshade image of post drainage terrain where the water exits the glacial drainage outlet, based on the 2021 0.1 x 0.1 m Wingtra DEM. The drainage thresholds show the highest elevation points along the drainage routes. The 2015 and 2021 ice margins are digitized based on the ArcticDEM and Mission I derived DEM, respectively. C) and D) Ice blocks deposited along the two drainage routes, up to 5 x 5 m in size. E) Water escape hole, 10 m in diameter. There is a total of five holes on the ice margin. F) Fractured ice due to supraglacial water flow. G) and H) Circular fractures on the ice originating from sub- or englacial water flow.

5 Discussion

5.1 Drainage volume estimates

220   For all GLOFs except 2014, the DEM and hydrograph based methods produce volume estimates located within each other's margins of error (Table 2, Figure 3) with a total mean difference of 10 % (excluding the 2014 event). This underlines that the two methods to obtain drained volumes serve as independent validation for one another. For the 2014 GLOF the hydrograph estimate is greater; two times as large as the DEM-derived volume. This could partly be due to the cloud-free Landsat 8 images captured closest to the drainage date on August 3 2014 is from July 21 2014, 13 days prior to the GLOF. Using the max 2010-

225   inflow rate of 1.3 m^3 s^{-1} (Russell et al., 2011), the lake volume would increase by approx. 1.5 M m^3, which is still 3.2 M m^3 lower than the hydrograph estimate. However, based on a comparison between the 2010 and 2014 July temperature at KAN_L the actual inflow rate is likely smaller, leaving the discrepancy between the two estimates even larger. It has been suggested that GLOFs can trigger additional release of meltwater from englacial storages or due to frictional melting (Huss et al., 2007; Mernild and Hasholt, 2009). This would show as larger hydrograph estimates and could explain the 2014 volume difference.

230   However, as all remaining GLOFs present no evidence of additional water release, it is considered unlikely. Moreover, we find no evidence of changes in lake area of any of the proglacial lakes in the system that could indicate changes in the water storage, and as such the 2014 event remains unreconciled

When the lake drains below the 2021 post-drainage DEM reference elevation of 408.8 m (2007, 2008, 2011-2015, 2018, 2020, 2021) we underestimate the volume release, as we cannot measure the precise post drainage water level. As annual differences

235   in the post-drainage area are minimal (Table 2), the changes in volume are also expected to be limited. Additionally, the total lake area during these instances is at its minimum. Russell et al., (2011) reported the post drainage water level of the 2007 event to be 404.5 m, which is 3.34 m lower than our 2021 reference minimum. Assuming that the entire 2007 post-drain area (Table 2) is lowered by an additional 3.34 m, it would give an extra volume release of 1.59 M m^3 corresponding to a 4 % increase from 37.73 M m^3 to 39.32 M m^3. Russell et al., (2011) estimated the volume of the 2007 event to be 39.1 M m^3.

240   Mernild & Hasholt (2009) and Mikkelsen et al., (2013) find much lower drainage volumes for the 2007 GLOF of 25.5 M m3 and 11.3 M m3, respectively (Table 2), however, these estimates are based on obsolete stage-discharge relations (van As et al., 2017). A similar pattern of matching and conflicting volume estimates is identified for other previous GLOFs (i.e, 2008, 2010, 2012, 2014, 2015 in Table 2), both across existing studies as well as compared to the reconstructed volumes of this study. This shows the challenges related to reconstructing drainage volumes and stresses the need for consistent methodological estimates

245   for a better comparison of yearly changes in the drainage parameters.

5.2 Drainage trigger mechanisms and controls

With the documentation of seven new and a re-calculation of seven known GLOFs showing variation in timing and magnitude, we are now able to re-evaluate proposed drainage triggering mechanisms. Previous studies have suggested various trigger mechanisms controlling the GLOFs at Russell Glacier such as flotation of the ice dam (Carrivick et al., 2017), fluctuation in

250   subglacial meltwater (Russell & de Jong, 1988; Russell, 1989), incomplete resealing of the subglacial conduit, and subglacial drainage through an incised bedrock-walled Nye channel (Russell et al., 2011). Recent data from ground penetrating radar revealed no evidence of any Nye channel incised into the bedrock but instead found evidence of at least one englacial tunnel running parallel to the ice margin (Lamsters et al., 2020).

Had the lake been draining due to floatation of the ice dam we would expect to see a gradual decrease in the release volume
255   and pre-drainage water level as less water is required to float the thinning ice dam. We do observe a lower drainage volume compared to the 2007 and 2010 maximum, but the lake is still able to drain at similar and higher water levels than observed in 2008 (Figure 3, Table 2). The two largest GLOFs (i.e. 2007 and 2010) both occurred following years of no drainages and indicate that in order for the lake to reach such high water level an additional (or multiple) melting season is required. However, due to the thinning of the damming glacier the lake is not able to reach its previous peak drainage water level and volume
260   observed in 2007 or 2010, and can, based on its current configuration, only reach a maximum water level of 433 m, at which point the lake overspills the ice dam.

Russell (1989) pointed to the internal drainage network of Russell Glacier and a possible reduction of (sub)glacial meltwater as the main trigger for the 1987 and 1984 GLOFs. This fits well with the majority of the observed GLOFs occurring late in the melt season when sub- and englacial water pressure is lower. However, the partial drainage events of 2014, 2015, 2017, and
265   2020 occur earlier in the melt season indicating a different drainage mechanism or another trigger for the lowering of the water pressure. The water pressure can also be lowered as a consequence of a sudden reduction in meltwater production (Tweed and Russell, 1999) and Russell et al. (2011) suggested a link to an observed drop in air temperature prior to the 2007 and 2008 GLOFs. For 7 of the 12 GLOFs occurring from 2010-2021 (2010-2011, and 2015-2019), we observe a similar drop in mean air temperature (MAT) when comparing the MAT of the 10 days prior to the GLOF with the MAT of the month prior (Figure
270   5). The difference ranges from -1.1 to -4.5 °C, with the largest drop observed in 2019. For the five remaining GLOFs the mean temperature changes are either very moderate (-0.2 - -0.5 °C) or increasing (0.3 - 1.1 °C). However, when comparing the 10-day MAT to the 5-day MAT prior to the drainage in both 2012 and 2013 we observe a 1.7 and 3 °C drop, respectively (Figure 5). A drop in temperature could influence the triggering of the GLOFs as the sub- and englacial water pressure falls in response to the reduced ablation and thereby permitting the lake water to escape via hydraulic connection to the englacial conduit. The
275   syphoning mechanism may be triggered by a reduction in melt, but as the timing and triggering threshold of the GLOF is linked to the water pressure dynamics of the englacial hydrological system it also reflects annual variations in the glacial drainage system (Tweed and Russell, 1999; Russell et al., 2011). As syphoning requires the draining lake to already be connected to the glacial drainage network (Tweed and Russell, 1999), a different mechanism must have triggered the 2007 GLOF and caused it to produce the englacial tunnel, which likely still acts as the main drainage passage for the following
280   yearly reoccurring events.

The fluctuation between short periods of relatively high and low drainage volumes (Figure 3, Table 2), points towards other factors also influencing the triggering threshold. The partial 0.9 M m^3 GLOF in 2020 drained just 0.3m ± 0.5 above the post drainage water level of the 11M m^3 2019 GLOF. This suggests that the ice dam did not seal during the 2019-2020 winter,

allowing the lake to drain already at the beginning of the ablation season in late May. We hypothesize, that the large GLOFs
285   potentially weaken the ice dam allowing the following event(s) to occur at much lower water level. A similar theory is
suggested by Russell et al. (2011) as explanation for the differences between the 2007 and 2008 events. After a few small
events the drainage system likely undergoes changes and the drainage outlet properly closes allowing for a reoccurrence of a
larger GLOF.

Figure 5. Plot of hourly temperature measurements from 10 days prior to the drainage event from KAN_L. Green line shows the mean air temperature (MAT) 41-10 days prior to the drainage, red line shows MAT 10-0 days prior, and orange line MAT 5-0 days prior to drainage. Red circle denotes the start of the GLOF and for the 2018 event the circle is larger due to uncertainty about the timing.

5.3 Evidence of changing drainage route

Previous observations of the lake drainage system (e.g. Carrivick et al., 2018; Mernild & Hasholt, 2009; Russell, 1989) coincides with the estimated drainage route I. In this study, the scattered ice blocks and the fractured ice surface observed in Fig. 4(B, C, D, F), indicate a considerable flow of surface water along both drainage route I and the new route II during the 2021 GLOF. The parallel, circular cracks on the ice margin (Figure 4B, 4G, 4H) were likely caused by a sudden drop in elevation which indicates a substantial amount of sub- or englacial drainage water flowing beneath the margin and thus undermining the surface structure of the glacier. The multiple water escape holes observed in figure 4B and 4E are either blowholes created as sub- or englacial pressurized water was forced upwards or they are simply collapsed ice roofs, both likely effects of sub- or englacial water flow.

From 3m Planet satellite images (Planet Team, 2017) captured immediately before and after the 2021 GLOF, we also observe geomorphological changes along the ice-marginal meltwater drainage system which channels the GLOF drainage water from drainage route II into the downstream river network. This observation caused us to check back through previous events, and whilst there is no evidence of geomorphological changes along the ice-marginal meltwater drainage system after the 2020 and 2019 events, we did observe standing water on the ice margin and changes in the ice colour (black to white) after the 2019 drainage, indicating water flow on the ice surface.

On the basis of these observations, we hypothesize that the new drainage pattern is caused mainly due to the thinning and retreat of the ice margin in the vicinity of the outlet allowing floodwater to more easily run over and into the ice margin. The 0.4 m elevation difference between drainage threshold 1 and 2 (Figure 4B) suggest that drainage route I is still the primary path. However, as the ice margin gradually thins the new additional drainage route II will become the dominant. This shift is very profound, because it bypasses the two outlet lakes (Figure 1) that currently acts as buffers and slow the downstream water flow. Thus, the shift will affect the downstream geomorphology and potentially cause hazards and we suggest a comprehensive study of the potential downstream consequences of floods along the new route is needed.

7 Conclusion

This study presents one of the longest and continuous known records of GLOF drainage estimates in Greenland. We (re)analyse 14 GLOFs spanning from 2007 to 2021 to provide a new evaluation and better understanding of drainage patterns and trigger mechanisms.

Our time series reveal yearly reoccurring GLOFs, with the exception of 2009, and considerable variations in both the drainage date ranging from May 31 to September 15, as well as volumes ranging from 0.9 to 37.7 M m^3. We compare lake drained volume estimates from DEM analyses with flood volumes calculated from a downstream hydrograph and find that the two methods produce comparable results with a mean volume difference of 10 %. That difference is excluding the 2014 GLOF where the hydrograph estimate is double the DEM-derived volume, which for now remains unresolved. In general, we find that our reconstructed time series illustrates the need for consistent methodological estimates when studying year-to-year

variations. We show that the 2021 theoretical maximum drainage volume is 14.3 M m^3 which is a 63 % decrease compared to the 37.7 M m^3 volume estimate for the 2007 GLOF. This decrease can be explained as due to an observed thinning of the ice dam.

325 We hypothesize that when the ice-dammed lake episodically drains suddenly, it does so through an englacial tunnel created by the 2007 GLOF. Ensuing annual sudden drainages are caused by a syphoning drainage mechanism within the pre-existing englacial conduit. The syphoning is likely triggered by a reduction in melt water, driven by late-season drainages and sudden reductions in mean air temperature, as well as due to annual variations in the internal drainage system of the damming glacier. The observed fluctuations between short periods of relatively high and low drainages volumes suggest that the large GLOFs

330 potentially weaken the ice dam causing it not to seal during winter and thus allowing the following event(s) to drain at a lower water level.

This study also reports geomorphological evidence from UAV and satellite data that reveals an altering of the proglacial drainage route with a new sub- or en- and supraglacial flow of drainage water going across the ice margin. We suggest that the new drainage route has developed due to a thinning and retreat of the ice margin and that a further thinning will cause the new

335 drainage route to eventually become dominant. As the new route bypasses the two buffering outlet lakes the delivery of drainage water to the downstream system will be faster and less attenuated, with large consequences for the geomorphology and a potential risk of flooding hazards.

Appendices
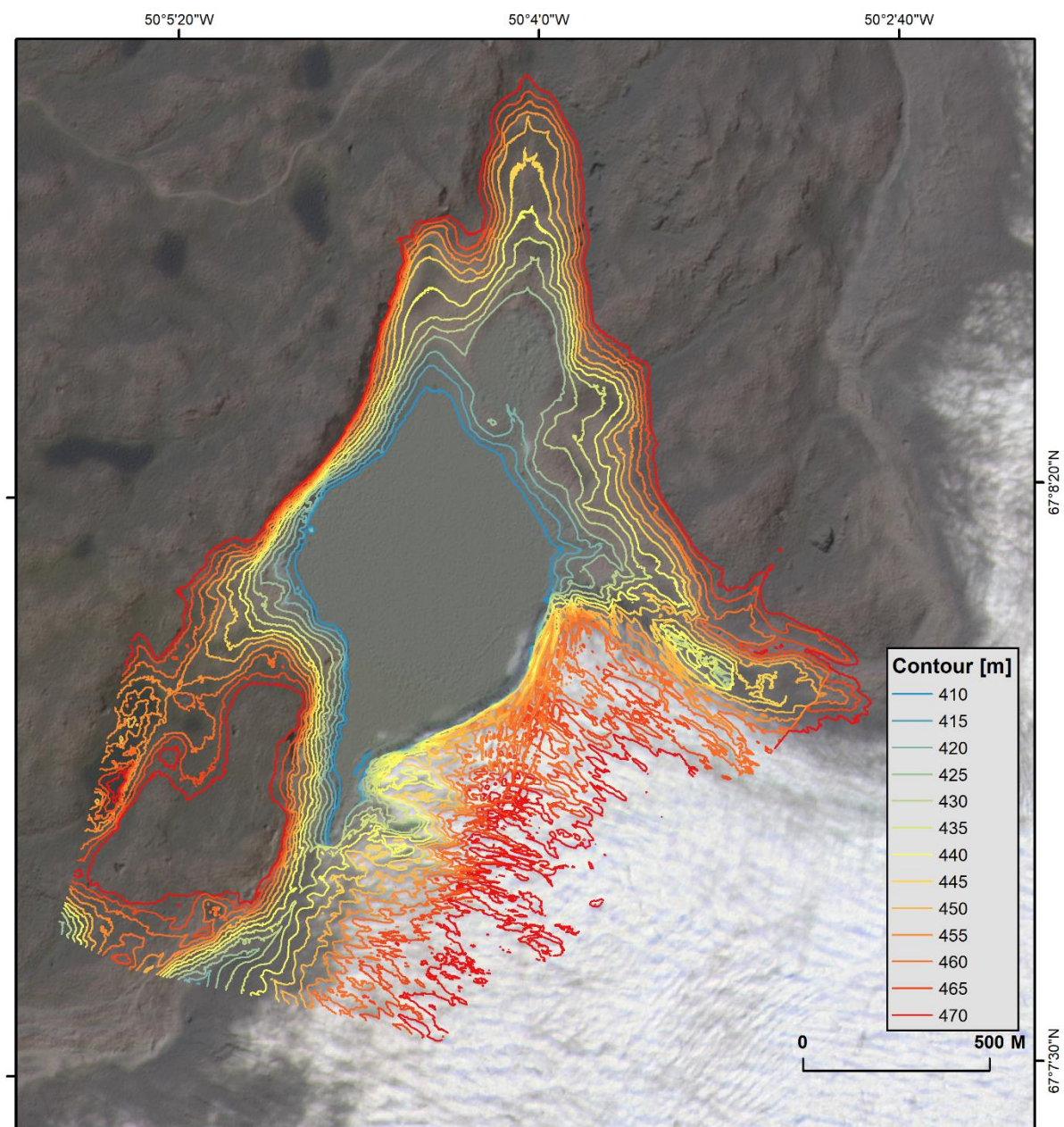
Figure A1. Contour map with 5 m intervals based on the 2021 post-drainage DEM shown on a Planet (2017) images.

340
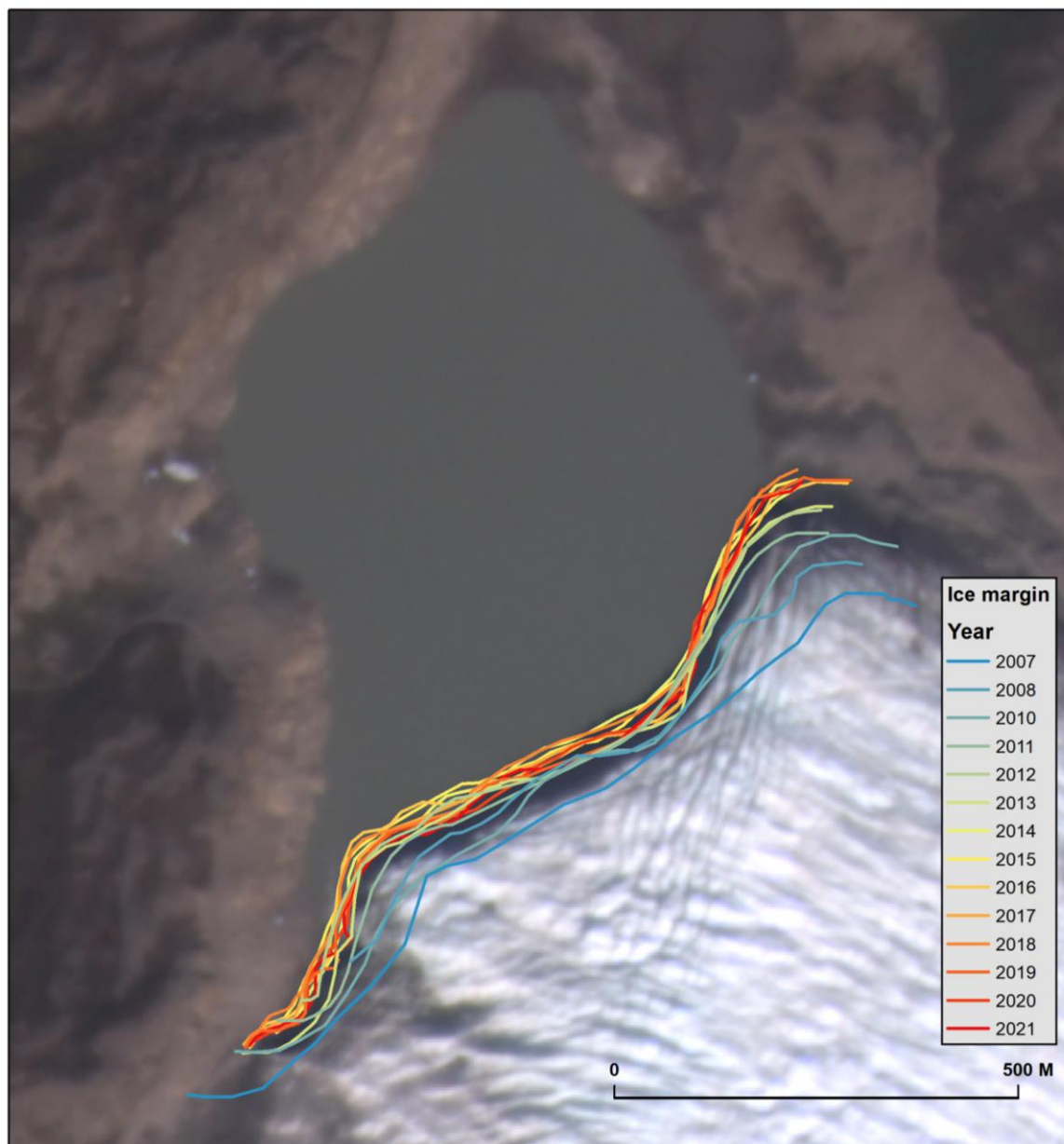
Figure A2. Position of ice margin digitized based on satellite images, shown on a Planet (2017) images.

Data availability

The UAV DEMs and orthophotos will be made available through Pangaea upon publication. DOI will be inserted here.

345 **Author contributions**

MD led the data analysis and wrote the main manuscript. MD, FH, AAB planned the study and carried out the fieldwork. KKK collected the hydrograph data and performed the hydrograph volume estimates. SAK carried out GPS data processing. JLC provided guidance on the interpretations and assessment of the drainage triggers and water rerouting. All authors contributed to the data analysis and interpretation of results and provided inputs for the manuscript.

350 **Competing interests**

The authors declare that they have no conflict of interest.

Acknowledgements

This work was funded by the Villum Foundation, Villum Young Investigator Grant no. 29456
Data from the Programme for Monitoring of the Greenland Ice Sheet (PROMICE) and the Greenland Analogue Project (GAP)
355 were provided by the Geological Survey of Denmark and Greenland (GEUS) at http://www.promice.dk

References

Agisoft LLC: Agisoft Metashape User Manual, 160, 2020.

van As, D., Mikkelsen, A. B., Nielsen, M. H., Box, J. E., Liljedahl, L. C., Lindbäck, K., Pitcher, L., and Hasholt, B.:
360 Hypsometric amplification and routing moderation of Greenland ice sheet meltwater release, 11, 1371–1386, https://doi.org/10.5194/TC-11-1371-2017, 2017.

Bevis, M., Wahr, J., Khan, S. A., Madsen, F. B., Brown, A., Willis, M., Kendrick, E., Knudsen, P., Box, J. E., van Dam, T., Caccamise, D. J., Johns, B., Nylen, T., Abbott, R., White, S., Miner, J., Forsberg, R., Zhou, H., Wang, J., Wilson, T., Bromwich, D., and Francis, O.: Bedrock displacements in Greenland manifest ice mass variations, climate cycles and climate
365 change, Proc Natl Acad Sci U S A, 109, https://doi.org/10.1073/pnas.1204664109, 2012.

Carrivick, J. L. and Quincey, D. J.: Progressive increase in number and volume of ice-marginal lakes on the western margin of the Greenland Ice Sheet, 116, https://doi.org/10.1016/j.gloplacha.2014.02.009, 2014.

Carrivick, J. L. and Tweed, F. S.: A global assessment of the societal impacts of glacier outburst floods, 144, https://doi.org/10.1016/j.gloplacha.2016.07.001, 2016.

370 Carrivick, J. L. and Tweed, F. S.: A review of glacier outburst floods in Iceland and Greenland with a megafloods perspective, https://doi.org/10.1016/j.earscirev.2019.102876, 2019.

Carrivick, J. L., Turner, A. G. D., Russell, A. J., Ingeman-Nielsen, T., and Yde, J. C.: Outburst flood evolution at Russell Glacier, western Greenland: Effects of a bedrock channel cascade with intermediary lakes, 67, 39–58, https://doi.org/10.1016/j.quascirev.2013.01.023, 2013.

375 Carrivick, J. L., Tweed, F. S., Ng, F., Quincey, D. J., Mallalieu, J., Ingeman-Nielsen, T., Mikkelsen, A. B., Palmer, S. J., Yde, J. C., Homer, R., Russell, A. J., and Hubbard, A.: Ice-dammed lake drainage evolution at russell glacier, west greenland, 5, 1–16, https://doi.org/10.3389/feart.2017.00100, 2017.

Carrivick, J. L., Yde, J. C., Knudsen, N. T., and Kronborg, C.: Ice-dammed lake and ice-margin evolution during the Holocene in the Kangerlussuaq area of west Greenland, 50, https://doi.org/10.1080/15230430.2017.1420854, 2018.

380 Chudley, T. R., Christoffersen, P., Doyle, S. H., Abellan, A., and Snooke, N.: High-accuracy UAV photogrammetry of ice sheet dynamics with no ground control, 13, 955–968, https://doi.org/10.5194/tc-13-955-2019, 2019.

Fausto, R. S., van As, D., Mankoff, K. D., Vandecrux, B., Citterio, M., Ahlstrøm, A. P., Andersen, S. B., Colgan, W., Karlsson, N. B., Kjeldsen, K. K., Korsgaard, N. J., Larsen, S. H., Nielsen, S., Pedersen, A., Shields, C. L., Solgaard, A. M., and Box, J. E.: Programme for Monitoring of the Greenland Ice Sheet (PROMICE) automatic weather station data, 13, 3819–3845,

385 https://doi.org/10.5194/ESSD-13-3819-2021, 2021.

Furuya, M. and Wahr, J. M.: Water level changes at an ice-dammed lake in west Greenland inferred from InSAR data, 32, https://doi.org/10.1029/2005GL023458, 2005.

GEUS Dataverse; https://doi.org/10.22008/promice/data/aws, last accessed 16 June 2022.

How, P., Messerli, A., Mätzler, E., Santoro, M., Wiesmann, A., Caduff, R., Langley, K., Bojesen, M. H., Paul, F., Kääb, A.,

390 and Carrivick, J. L.: Greenland-wide inventory of ice marginal lakes using a multi-method approach, 11, https://doi.org/10.1038/s41598-021-83509-1, 2021.

Huss, M., Bauder, A., Werder, M., Funk, M., and Hock, R.: Glacier-dammed lake outburst events of Gornersee, Switzerland, 53, https://doi.org/10.3189/172756507782202784, 2007.

Kjeldsen, K. K., Mortensen, J., Bendtsen, J., Petersen, D., Lennert, K., and Rysgaard, S.: Ice-dammed lake drainage cools and

395 raises surface salinities in a tidewater outlet glacier fjord, west Greenland, 119, https://doi.org/10.1002/2013JF003034, 2014.

Kjeldsen, K. K., Khan, S. A., Bjørk, A. A., Nielsen, K., and Mouginot, J.: Ice-dammed lake drainage in west Greenland: Drainage pattern and implications on ice flow and bedrock motion, 44, https://doi.org/10.1002/2017GL074081, 2017.

Lamsters, K., Karušs, J., KrievÄans, M., and Ješkins, J.: High-Resolution Surface and Bed Topography Mapping of Russell Glacier (Sw Greenland) Using Uav and Gpr, in: ISPRS Annals of the Photogrammetry, Remote Sensing and Spatial

400 Information Sciences, 757–763, https://doi.org/10.5194/isprs-annals-V-2-2020-757-2020, 2020.

McNabb, R.; Pybob: A Python Package of Geospatial Tools; Github, 2019

Mernild, S. H. and Hasholt, B.: Observed runoff, jökulhlaups and suspended sediment load from the Greenland ice sheet at kangerlussuaq, west Greenland, 2007 and 2008, 55, https://doi.org/10.3189/002214309790152465, 2009.

Mikkelsen, A. B., Hasholt, B., Knudsen, N. T., and Nielsen, M. H.: Jökulhlaups and sediment transport in watson river, 405   kangerlussuaq, west greenland, 44, 58–67, https://doi.org/10.2166/nh.2012.165, 2013.

Noh, M. J. and Howat, I. M.: Automated stereo-photogrammetric DEM generation at high latitudes: Surface Extraction with TIN-based Search-space Minimization (SETSM) validation and demonstration over glaciated regions, 52, 198–217, https://doi.org/10.1080/15481603.2015.1008621, 2015.

Nuth, C. and Kääb: Co-registration and bias corrections of satellite elevation data sets for quantifying glacier thickness change, 410   5, 271–290, https://doi.org/10.5194/tc-5-271-2011, 2011.

Planet Team; Planet Application Program Interface: In Space for Life on Earth, San Francisco, CA, 2017

Russel, Andrew. J. and de Jong, C.: Lake drainage mechanisms for the ice-dammed oberer russellsee, Søndre Strømfjord, West Greenland, Zeitsch, 24, 143–147, 1988.

Russell, A. J.: A comparison of two recent jokulhlaups from an ice-dammed lake, Sondre Stromfjord, West Greenland, 35, 415   https://doi.org/10.3189/s0022143000004433, 1989.

Russell, A. J.: Controls on the sedimentology of an ice-contact jökulhlaup-dominated delta, Kangerlussuaq, west Greenland, 193, https://doi.org/10.1016/j.sedgeo.2006.01.007, 2007.

Russell, A. J., Carrivick, J. L., Ingeman-Nielsen, T., Yde, J. C., and Williams, M.: A new cycle of jö kulhlaups at Russell Glacier, Kangerlussuaq, West Greenland, 2011.

420   Shugar, D. H., Burr, A., Haritashya, U. K., Kargel, J. S., Watson, C. S., Kennedy, M. C., Bevington, A. R., Betts, R. A., Harrison, S., and Strattman, K.: Rapid worldwide growth of glacial lakes since 1990, 10, https://doi.org/10.1038/s41558-020-0855-4, 2020.

Sugiyama, S., Bauder, A., Weiss, P., and Funk, M.: Reversal of ice motion during the outburst of a glacier-dammed lake on Gornergletscher, Switzerland, 53, https://doi.org/10.3189/172756507782202847, 2007.

425   Tweed, F. S. and Russell, A. J.: Controls on the formation and sudden drainage of glacier-impounded lakes: implications for jökulhlaup characteristics, Progress in Physical Geography, 79–110 pp., 1999.